Insights into migration and transformation of Cu Species during SO_2 Poisoning and Hydrothermal Aging of Cu/SAPO-34 NH_3-SCR Catalysts

Fumei Wang,[a] Qi Cai,[a] Xinhua He,[a] Boxiong Shen,[a]* Leila Negahdar,[b] Shuo Feng[a] and Andrew M. Beale[c]*

ABSTRACT: Cu/SAPO-34 catalysts have been widely used for NOx reduction from diesel exhaust by ammonia-SCR. Sulfur poisoning remains a challenge for Cu/SAPO-34 catalysts in NH_3-SCR, restricting its application. In this study, Cu/SAPO-34 samples containing a mixture of Cu species comprising isolated Cu^{2+} located in the 6MR, $Cu(OH)^+$ in 8MR, CuO clusters/nanoparticles and Cu^+ species were prepared. The Cu speciation during SO_2 and hydrothermal aging of Cu/SAPO-34 SCR catalysts was subsequently studied. Whilst hydrothermal aging had little effect on catalytic activity, the sulfur aged sample exhibited deterioration in NH_3-SCR activity over the temperature range 100–575 °C. The breakage and collapse of the zeotype framework and chemical deactivation of Cu/SAPO-34 catalyst after expose to SO_2 and H_2O took place. A combination of XPS and TGA-DT-DSC revealed the presence of ammonium bisulfate, copper bisulfate/sulfate, aluminium sulfate and sulfuric acid after SO_2 and H_2O co-poisoning under SCR conditions. Furthermore, $Cu(OH)^+$ tended to migrate to form isolated Cu^{2+} and Cu^+, as well as agglomerating to form CuO particles. DFT calculations revealed SO_2 and O_2 can readily absorb on CuO particle to form stable copper bisulfate/sulfate species with the following order of preference: CuO > Cu^+> Cu^{2+}> $Cu(OH)^+$. In contrast, $Cu(OH)^+$ was less prone to be poisoned by easily releasing SO_3 than other Cu specie sites.

1. INTRODUCTION

Selective catalytic reduction with NH_3 commonly abbreviated to NH_3-SCR, is an effective method to eliminate NOx from diesel exhaust. In particular, catalysts possessing the CHA topology including Cu/SSZ-13 and Cu/SAPO-34 have been shown to be effective catalysts for NO_X reduction to N_2 with a high selectivity, over a wide operating temperature window, whilst retaining outstanding hydrothermal stability and excellent hydrocarbon (HC) resistance.[1-4] Besides the SCR performance, improving the tolerance of SCR catalysts to poisoning caused by contaminants in the exhaust from diesel engines remains a challenge in NH_3-SCR technology. Cu-SAPO-34 has been found to display unexpected severe durability issues when exposed to water at low temperatures(<100 °C) [5,6], and sulfur poisoning is particularly problematic since copper ions can readily coordinate to S-containing molecules.[7,8]

The impact of SO_2 poisoning over copper-based chabazite (Cu-CHA) has been extensively investigated, with SO_2 poisoning of Cu−CHA zeolites proposed to decrease activity due to the formation of both ammonia sulfate at low temperature,[9,10] and copper sulfates. [11, 12] It has been shown that ammonium sulfate can decompose at temperatures over 350 °C and is therefore a reversible deactivation.[11] However, the copper sulfate species are more harmful to Cu-CHA catalysts, because the activity of the poisoned sample can only be partially recovered at high temperature (>550 °C) and as such can be considered a hard-reversible or an irreversible deactivation process.[11-13] Therefore, the irreversible deactivation mechanism for SO_2 poisoning is believed to be correlated with the copper sites, with Cu-sites bound to one bisulfate anion or Cu-ions surrounded by SO_4-ions.

Moreover, previous studies have reported that the responses of copper sites over Cu-CHA catalysts toward SO_2 poisoning are site-dependent.[9, 14, 15] Recent research identified that there are two distinct Cu cationic species brought about by ion-exchange: ion-exchanged Cu^{2+} ions (Z2Cu) in 6-membered rings (6MR) and $[Cu^{II}(OH)]^+$(ZCuOH) in the 8-membered rings (8MR).[14, 16] Shih *et al*.[17] found that Z2Cu sites are more resistant to SO_2-poisoning than ZCuOH sites in Cu-SSZ-13, revealing that Cu sites bound to one HSO_4^- are immobile, but

liberate from the framework and become more mobile when bound to two HSO_4^-. A similar result was obtained by Wang *et al*.[15] demonstrating that ZCuOH is the more vulnerable species to SO_2 poisoning. The isolated Cu^{2+} in 6MR is less susceptible to SO_2 poisoning because of its stronger interaction with the zeolite framework, while SO_2 can readily interact with $[Cu^{II}(OH)]^+$ to generate Cu-SO_4-like species deactivating the Cu active sites.

However, Wang *et al*.[15] reported that SO_2 interacted with ZCuOH and also interacted somewhat with the Z2Cu sites. Jangjou *et al*.[11] reported that the Cu^{2+} inside the 6MR was completely blocked by sulfur and that the nature of the $[CuOH]^+$ close to the 8MR changed over Cu-SSZ-13. It has also been reported that the amount of isolated Cu^{2+} declined significantly after SO_2 exposure according to EPR spectroscopy and *in situ* DRIFTS,[18] agreeing well with the results by Tang *et al*.[19] Luo *et al*.[9] also revealed that Cu sites could be tuned by hydrothermal aging and sulfur exposure, with NH_3 absorption on both Z2Cu and ZCuOH species decreasing after sulfur poisoning, the latter species being particularly more difficult to recover. Yong *et al*.[20] found that the interaction of Cu^{2+} with SO_2 resulted in the formation of $ZCuHSO_4$, which helped suppress the aggregation of Cu^{2+} into CuO and maintained more isolated Cu^{2+}, leading to higher activity at high temperatures. Moreover, it is also been shown by Hammershøi et al. using DFT calculations,[21] that SO_2 interacts more strongly with Cu^+ than Cu^{2+}, whilst Yang *et al*.[7] used DFT to determine that SO_2 tends to adsorb on Cu^+ and Cu^+/H^+ sites of Cu-SAPO-34. Since the NH_3-SCR process operates on a redox cycle, the oscillation between Cu^{2+} and Cu^+ oxidation states suggests that enhanced sulfur poisoning is a particular problem during reduction, particularly since the re-oxidation of Cu^+ is thought to be the rate-determining step of NH_3-SCR reaction.[22] However, Wang *et al*.[15] found Cu/SSZ-13 experiences a loss of activity at high temperature, which was attributed to newly formed CuOx clusters An investigation by Wei *et al*.[24] also showed that Cu-SO_4-like species increased in quantity after the hydrothermal aging at 850 °C and SO_2 poisoning over Cu-SSZ-13 catalyst and that this was due to the formation of inactive $CuO_X/CuAlO_X$, which was in agreement with the conclusion by Zhang *et al*..[23] Summarising, Cu-zeolite samples are known to contain multiple Cu-containing species, including ZCuOH, Z2Cu sites, CuO clusters/particles and Cu^+ species, which exhibit an ability to remove NO. It follows then that different Cu species on Cu-CHA zeolites & zeotypes show a different propensity to interact with S-containing compounds and subsequently result in different Cu-sulfur containing species.

Clearly, there is an urgent need to understand the migration and transformation of Cu species on poisoning as most types of Cu species were active for SCR reactions. In this work, Cu/SAPO-34 with different Cu species (including isolated Cu^{2+} located in the 6MR, $Cu(OH)^+$ in 8MRs, CuO and Cu^+) were prepared and tested under standard SCR conditions and further characterized to understand the role of Cu species during sulfur and water poisoning. The migration and transformation of Cu species during sulfation was studied and the mechanism for the interaction of SO_2 with O_2 and copper species was proposed. DFT calculations were subsequently performed to elucidate the Cu species and to determine their properties in order to support the experimental observations. The results from these studies provide insights into the mechanism of sulfur poisoning, facilitating the rational design and development of efficient catalysts in future practical NH_3-SCR in systems.

2. EXPERIMENTAL

2.1 Catalyst preparation. Cu/SAPO-34 sample with Cu mass fraction of 3 wt. % were prepared by combining the two-step liquid ion-exchange method with an impregnation method.[25,26] First, commercial H/SAPO-34 powder with mole ratio of P_2O_5:Al_2O_3:SiO_2=1:1:0.5 (Nankai University Catalyst, Tianjin, China) was ion-exchanged using NH_4NO_3 (99 % NH_4NO_3, Aladdin, China). Cu ion-exchange to obtain a 2 wt.% Cu loading was performed by mixing the NH_4-SAPO-34 with a $Cu(CH_3COO)_2$ solution at 60 °C for 4 h, forming Cu@SAPO-34 sample. Second, successive loading of another 1 wt.% copper into SAPO-34 was carried out through impregnation using a certain concentration of $Cu(NO_3)_2$ solution as copper precursor and the obtained Cu@SAPO-34 as support. Finally, the slurry was dried at 80 °C for 12 h while stirring and then calcined at 550 °C for 3.5 h, producing Cu/SAPO-34 sample. A final Cu content of 2.86 wt. % was determined by atomic absorption spectroscopy (AAS, Shimadzu) measurement.

The fresh Cu/SAPO-34 catalysts (Cu/SAPO-34-F) were hydrothermally aged at 750 °C for 24 h in a quartz tube reactor with 10 vol. % H_2O under SCR conditions (NH_3=NO=500 ppm, O_2=5 vol. %, balanced with N_2). The gas hourly space velocity (GHSV) was held at 120,000 h^{-1}. Then the catalysts were dried at 120 °C for 5 h to remove excess water, and the obtained samples were labeled as Cu/SAPO-34-HA. The Cu/SAPO-34-HA catalyst was further treated with sulfur dioxide exposure, which was conducted in 5 vol. % H_2O and 200 ppm SO_2 at 400 °C for 24 h under SCR

conditions (72 mg SO_2/g catalyst). Then the catalysts were dried at 120 °C for 5 h, and the hydrothermal aged and sulfated samples were labelled as Cu/SAPO-34-HSA, investigating the synergistic deactivation mechanism of hydrothermal aging and SO_2 poisoning. For comparison, sulfur poisoning of the Cu/SAPO-34 catalyst, denoted as Cu/SAPO-34-SA, was prepared in 200 ppm SO_2 in SCR atmosphere at 400 °C for 24 h. Beforehand, the fresh sample was first pretreated at 100 °C for 30 min in N_2.

2.2 Catalyst characterization. The morphology of the samples was determined using scanning(transmission) electron microscopy (SEM/STEM, Phenom pure plus, Netherlands). The BET specific surface area and pore volume analysis were carried out on an ASAP 2020 Micromeritics system. X-ray diffraction (XRD) was performed on a Bruker D8 FOCUS X-ray powder diffractometer employing Cu Kα radiation (λ = 0.15418 nm) with the 2θ range of 5-60 °. Temperature-programmed desorption of NH_3 (NH_3-TPD) and Temperature-programmed reduction by H_2 (H_2-TPR) were carried on a Chemical adsorption analyzer PCA-1200 (Beijing Builder Electronic Technology Co., Ltd) with a TCD detector. The mass of the catalyst sample studied was 100 mg. The flow rate of the analyzer was set to 30 mL/min (STP). The catalyst sample was first pretreated at 500 °C for 30 min in N_2. During the TPD/TPR process, the temperature was heated up to 600/900 °C with a heating rate of 10 °C/min in the same gas feed. The total acidity of the catalysts was obtained by an acid-alkali titration in which NH_3 was desorbed using HCl and NaOH solution. X-band Electron paramagnetic resonance (EPR) spectra were recorded on a Bruker ESP320 instrument. Before measurement, the samples were preheated in vacuum from room temperature to 120 °C for 5 h. The samples were then cooled to room temperature and X-band (υ = 9.78 GHz) spectra were recorded with the magnetic field sweeping from 2000 to 4000 G. Quantification of isolated Cu^{2+} was done by using standard solutions of copper (II) sulfate pentahydrate (at -150 °C). All EPR spectra of Cu/SAPO-34 catalysts were obtained at -150 °C. The UV–vis spectra were conducted on the Cary Series UV–Vis-NIR Spectrophotometer (Agilent Cary 5000) equipped with a diffuse reflectance accessory covering a bandwidth of 200–800nm. Thermal gravimetric analysis (TGA-DTG-DSC) of the catalyst samples was performed using TGA/SDTA851e (TA Instruments-Waters LLC) from room temperature to 1000 ℃ in air (50 mL/min) at a heating rate of 10 ℃/min with 10 mg samples. The accuracy of the instrument was determined to be 0.1 μg. For the TGA experiments, the spent catalyst samples were measured under from room temperature to 900 ℃ at

the heating rate of 10 ℃ min^{-1}. The DSC thermograms were analyzed by calculating as the area under the decomposition exothermic peak. The X-ray Photoelectron Spectroscopy (XPS, Shimadzu Kratos Ltd., JPN) was conducted to determine atomic concentrations and valence state of Cu and S elements in the catalysts. The spectrometer is equipped with Al-K_α radiation source. Prior to the analysis, the powder samples were heated at 100 °C for 2 h and were then reserved in N_2 flow.

2.3 Catalyst performance tests. The performance of the SCR catalysts were tested in a fixed-bed quartz reactor at 100~575 °C. The simulated flue gas composition was set as follows with total gas flow 1,000 mL/min, including NH_3=NO=500 ppm, O_2=5 vol. %, N_2 as equilibrium gas, with the weight of the catalyst was about 0.5 g, which was corresponded to the space velocity (GHSV) of 120,000 h^{-1}. The NO concentrations in the inlet gas and outlet gas were tested with a flue gas analyzer (KM940).

NO conversion was calculated according to the following formula:

$$\text{NO conversion efficiency}=\frac{NO_{in}-NO_{out}}{NO_{in}}\times 100\ \% \quad (1)$$

2.4 Theoretical calculations. The calculations were based on density functional theory (DFT) using projector augmented wave (PAW) methods, as implemented in the Vienna *ab initio* simulation package (VASP).[14] A plane-wave basis set with a kinetic-energy cut-off of 400 eV was used to expand the wave function of valence electrons. The generalized gradient approximation (GGA) with the Perdew-Burke-Ernzerhof (PBE) functional was used for describing the exchange-correlation interactions.[17] Here, we constructed isolated Cu^{2+} (located in 6MR sites), $Cu(OH)^+$ (located in 8MR sites), CuO (cluster on surface of SAPO-34) and Cu^+ (intermediate state, from Cu^{2+} reduced by the standard SCR process) structures supported on 2×1×1 supercell of SAPO-34 framework to simulate several different copper species in the experiment. The structural relaxations were performed by computing the Hellmann–Feynman forces within the total energy and force convergences of 10^{-4} eV and 0.05 eV/Å, respectively. The Brillouin-zone integration was sampled with 3 × 3 × 1 k-points Monkhorst-Pack mesh. In order to search transition states, the climbing image nudged elastic band method (CNEB, embedded in VASP) was employed.[14] A series of sulfur-related reactions with reference to gas-phase SO_2(including $*SO_2$ and *OSO structures) were studied. The binding energy was calculated according to the following equation:

$$\Delta E = E_{*M} - (E_* + E_M) \quad (2)$$

where E_{*M} and E_{*} were the total energy of basal with and without molecular M (M = SO_2), respectively.

3. RESULTS AND DISCUSSION

3.1 NH_3-SCR activity. NO conversion during NH_3-SCR for catalysts operating at 100 – 600 °C are shown in Fig. 1 The SCR activity of all catalysts was very limited below 150 °C. For the Cu/SAPO-34-F, Cu/SAPO-34-SA and Cu/SAPO-34-HA catalysts, NO conversion rapidly enhanced with increasing reaction temperature from 175 – 400 °C, reaching 99 % at 200 °C and maintaining high conversion levels up to 400 °C. NO conversion in the high temperature range (> 425 °C) decreased rapidly for all catalysts (falling to below 65 % at 600 °C). However, the NO conversion of all three aging samples decreased compared with fresh Cu/SAPO-34, while the Cu/SAPO-34-HSA exhibited a significant decline in NH_3-SCR performance, although it still reached 90 % NO conversion between 250 °C to 400 °C. This indicated that there were synergistic poisoning effects on catalytic activity between SO_2 exposure and hydrothermal aging. In addition, N_2 selectivity was studied and shown in Supporting Information section 1 (SI S1), and demonstrated that the fresh and hydrothermal aging catalysts showed relatively high N_2 selectivity over 90% over a broad temperature range 175-575 °C.

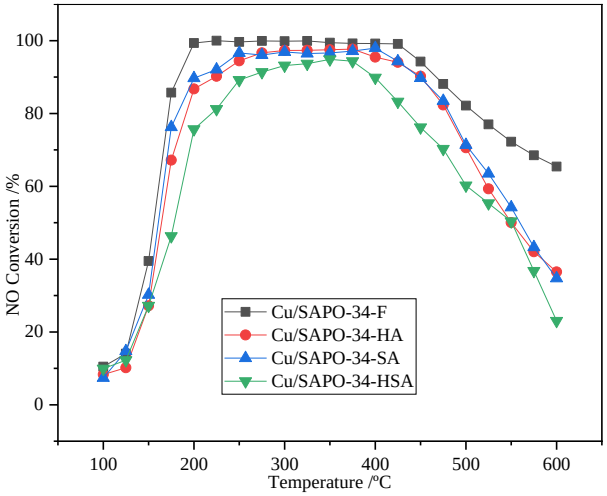

Figure 1. NO conversion over fresh and aging samples. Reaction Conditions: 500 ppm NO, 500 ppm NH_3, 5vol.% O_2, 3vol.% H_2O, 400ppm SO_2, balance N_2; GHSV=120,000 h^{-1}.

3.2 Crystal structure and morphology. 3.2.1 BET and pore structure. The BET surface area, pore volume and pore size results were shown in Table 1. It can be seen that the surface areas of Cu/SAPO-34-F and Cu/SAPO-34-HA catalysts were 412 m^2/g and 420 m^2/g, respectively. This is

similar with the results of 364 m^2/g and 456 m^2/g for fresh Cu/SAPO-34 samples by Wang *et al*.[27] The surface areas of the Cu/SAPO-34-SA catalyst was observed to slightly decrease whilst for the Cu/SAPO-34-HSA catalyst it declined significantly to 352 m^2/g, indicating that the hydrothermal and sulfur co-poisoning was detrimental to the physical properties of Cu/SAPO-34. This is further borne out by an analysis of the pore volume and size which were also observed to decline somewhat in the Cu/SAPO-34-SA and particularly for Cu/SAPO-34-HSA. These observations indicated that the presence of SO_2, particularly under hydrothermal conditions had significant synergistic poisoning effects on the pore structure and BET surface area of the catalysts.

Table 1 Specific surface area, pore volume and pore size of samples.

Samples	BET ($m^2 \cdot g^{-1}$)	Pore volume ($cm^3 \cdot g^{-1}$)	Pore size (nm)
SAPO-34	501	0.35	1.81
Cu/SAPO-34-F	412	0.25	1.83
Cu/SAPO-34-HA	420	0.25	2.51
Cu/SAPO-34-SA	401	0.24	1.73
Cu/SAPO-34-HSA	352	0.18	1.53

3.2.2 SEM-EDS mapping. The SEM images shown in SI Fig.S2, demonstrate that all samples exhibited the representative cubic structure of CHA. However, the blockage among the samples Cu/SAPO-34-SA and Cu/SAPO-34-HSA samples, suggested that pore plugging has occurred. In addition, some of the Cu/SAPO-34-HSA crystals had fractured into particles. This indicated that the presence of SO_2 and hydrothermal conditions led to damage to the pore structure and framework of the zeolites. The SEM-EDS patterns of fresh and aged Cu/SAPO-34 catalysts were obtained to investigate any morphological change and differences in elemental distribution and representative images from the catalysts are shown in Fig. 2. All catalysts showed the typical cubic crystals of CHA and that these were of the order of a few (2-3) μm in size. The Cu/SAPO-34 samples before and after hydrothermal aging appear to retain a uniform and homogeneous distribution of elements in the crystals, likewise with the Cu/SAPO-34-HA sample. After sulfur poisoning treatment under hydrothermal conditions, however, the surface morphology and structure of the Cu/SAPO-34-HSA samples alters with voids seen in the crystal as well as damage to the crystal periphery observed, where a hole was indeed introduced into the crystals of the Cu/SAPO-34-HAS, which also appears consistent with the conclusions of the SEM images. Shan *et al*.[28] proposed that SO_2 could dislodge

extra-framework Al ions caused by the dealumination process brought about by hydrothermal aging in the presence of SO_2.

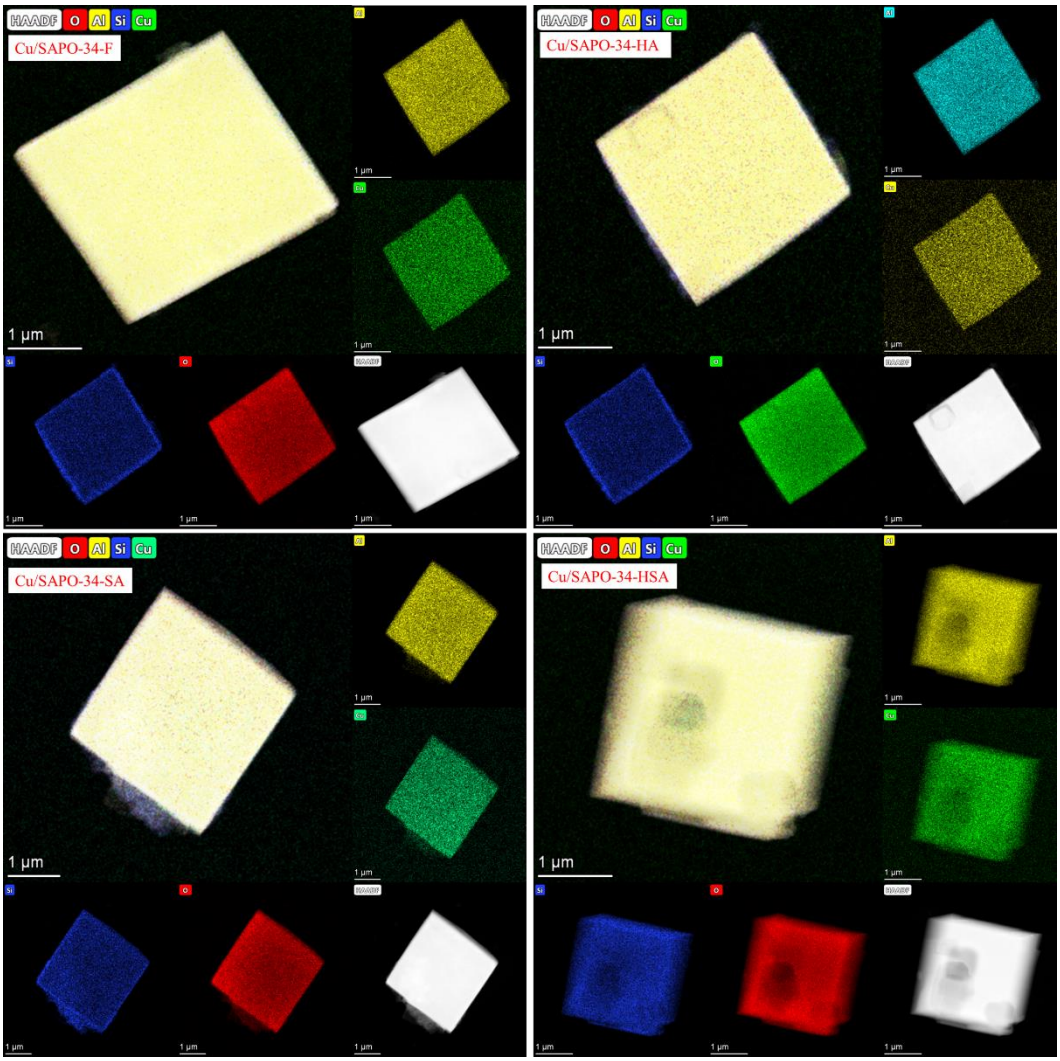

Figure 2. High-Angle Annular Dark Field (HAADF) and elemental Element mapping images distribution on the Cu/SAPO-34 samples before and after treatment.

3.2.3 XRD. XRD patterns were shown in Fig. 3, with the fresh Cu/SAPO-34 sample exhibiting the typical reflections of the SAPO-34 CHA topology (2θ = 9.6, 12.9, 16.1, 20.7, 25.9 and 30.9 °) with a high degree of crystallinity assigned, agreeing well with previously reported patterns of SAPO-34 in the literature.[25, 29] The XRD patterns recorded for the Cu/SAPO-34-HA sample were similar to that of Cu/SAPO-34-F sample, albeit exhibiting a partial loss of crystallinity. However, it should be noted that a significant decrease in reflection intensity was observed for Cu/SAPO-34-SA and Cu/SAPO-34-HSA samples, indicating loss of the structural crystallinity or else significant filling of the micropore volume. This was consistent with the decreasing trend in pore volume and BET surface area of the Cu/SAPO-34-SA and Cu/SAPO-34-HSA samples as blockage happened

among crystals in SEM. However, as with the data presented here, there was no evidence of diffraction intensity ascribed to the presence of crystalline Cu-containing phases and therefore any copper content present is well-dispersed on the surface of the zeotype structure.[2, 24]

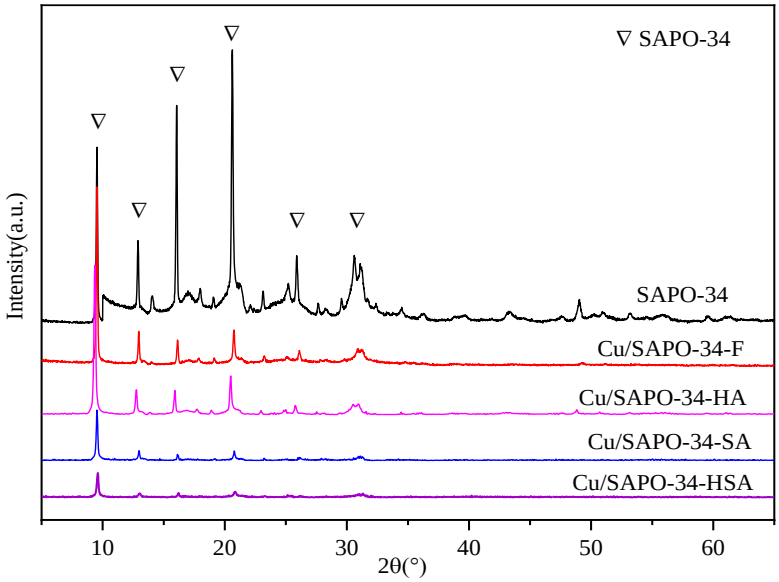

Figure 3. XRD patterns of the Cu/SAPO-34 samples before and after treatment.
Note the decreasing intensity of the reflections due to various hydrothermal/SO_2 treatments.

3.3 Migration of Cu species. 3.3.1 Surface acidity. NH_3-TPD experiments have been carried out to determine the acid properties of the samples and the results are shown in Fig. 4. All catalysts showed similar NH_3 desorption curves with two main NH_3 desorption peaks, a low temperature peak centered at 186 °C, representing the NH_3 desorbed from Lewis acid sites/condensed ammonia, and an intermediate temperature broad peak centered at 305 °C, previously assigned to NH_3 adsorbed on strong Brønsted acid sites (Si-OH-Al and Cu^{2+} sites).[1, 30] It was noted that the Cu/SAPO-34-HSA sample exhibited a broader NH_3 desorption peak in the temperature range extending from 250–500 °C whilst the sample also possessed the greatest acid content ~2.61 mmol/g from Table 2. This result was different from that reported by Shan *et al*. [28] where it was observed the total number of acid sites decreased sharply after sulfur poisoning due to dealumination. Here it was observed a different effect caused by the introduction of the SO_2 and H_2O suggesting the presence of sulfur-containing species causing an increase in sample acidity.

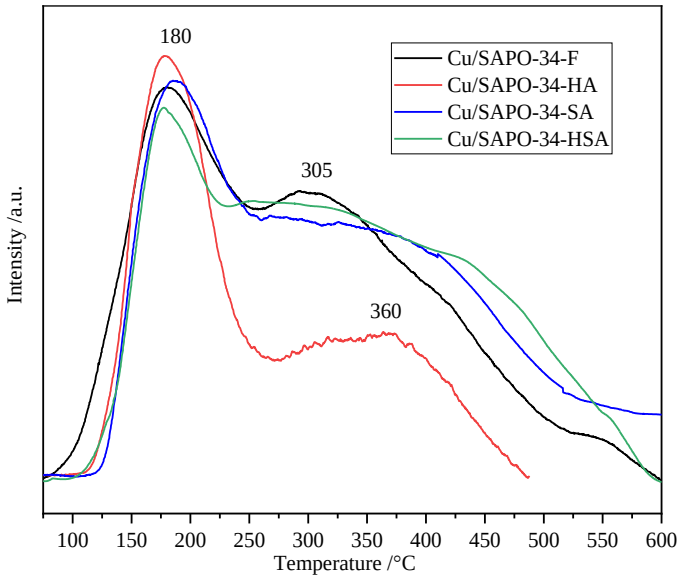

Figure 4. NH_3-TPD results of samples of the Cu/SAPO-34 samples before and after various treatments.

Table 2 Total acid quantity of samples derived from the data shown in Fig. 4.

Samples	Total acid quantity(mmol/g)
Cu/SAPO-34-F	2.54
Cu/SAPO-34-HA	2.28
Cu/SAPO-34-SA	2.57
Cu/SAPO-34-HSA	2.61

3.3.2 Redox feature. H_2-TPR measurements were carried out to determine the nature of Cu species and the results are shown in Fig. 5. The H_2 consumption peaks observed from 175 °C to 650 °C indicate that multiple Cu species coexist in all samples. The peak located at lower temperatures (centered at 230–270 °C) has previously been assigned to the reduction of $Cu(OH)^+$ to Cu^+ whereas the peak at the moderate temperature (centered at 300–344 °C) assigned to the reduction of CuOx.[25, 29, 31, 32] The peak at 355-398 °C had previously been assigned to the reduction of isolated $Cu^{2+} \rightarrow Cu^+$.[29, 30, 32, 33] We propose that the peak around 496-522 °C in Cu/SAPO-34-SA and Cu/SAPO-34-HSA may stem from the reduction of Cu-aluminate like species (eg. CuAlOx).[31, 33-35] Hence, this means there could be at least three different types of copper species, which were $Cu(OH)^+$, bulk CuOx species, and isolated Cu^{2+}. However, after hydrothermal aging and sulfur exposure, it is obvious that the $Cu(OH)^+$ species decreased, while isolated Cu^{2+} only changed slightly. Interestingly, it appeared that CuO species were observed to decrease and stable Cu^+ ions from Cu-aluminate like species was found after H_2O and SO_2 introduction. It is indicated that CuO species may be more likely to be harmed by co-exist H_2O and SO_2.

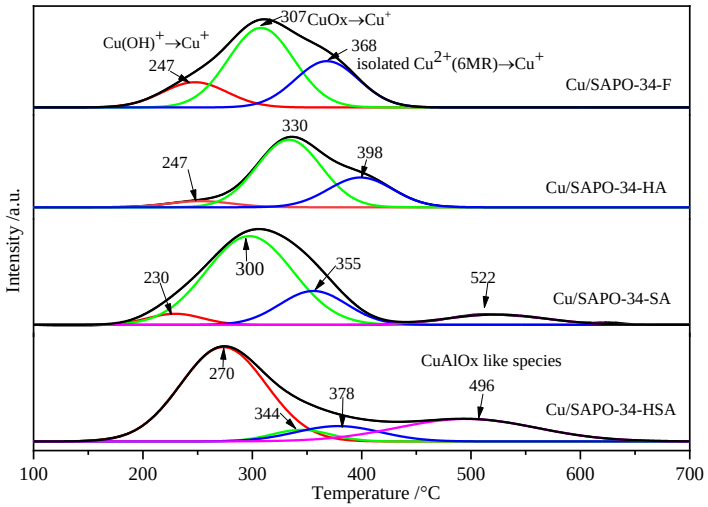

Figure 5. H_2-TPR results of samples of the Cu/SAPO-34 samples before and after various treatments.

3.3.3 XPS. The XPS spectra of all samples was shown in Fig. 6. It displayed that the main Cu 2p peak was fitted with two contributions at 932.2 eV corresponding to Cu^+ species and at 934.5 eV to Cu^{2+} species, and the former can be tentatively assigned to Cu_2O.[36,37] And the relative content of Cu species was calculated, as shown in Table 3. The Cu species on the fresh samples and hydrothermal aging samples were almost indistinguishable. However, the rate of Cu^+ with 11.4 % species increased to 32 % due to Cu^{2+} reduction after sulfur poisoning treatment compared with fresh samples. Based on H_2-TPR, this was a powerful evidence that the Cu^+ was obtained from Cu^{2+} reduction as the redox behavior is the core step of Cu-SAPO-34 catalyst for NO removal. Yang *et al.*[7] found that Cu^+ and Cu^+/H^+ sites were favorable sites for SO_2 adsorption. Similar observations were disclosed that SO_2 adsorbed more strongly on Cu^+ than on Cu^{2+},[21] and highly mobile Cu^+ species showed a predominant influence on NH_3-SCR sensing at low reaction temperatures.[38] The Cu species was also investigated by EPR spectra and UV–vis spectrum in SI S3 & Fig.S4. The results showed that there were Cu^{2+}, Cu^+ and CuO species in fresh Cu-SAPO-34 catalysts, and it also confirmed the Cu^{2+} species migrated during hydrothermal aging and sulfur poisoning.

After undergoing sulfur poisoning at 400 °C, additional sulphates were formed as compared to a SO_2 dynamic spent catalyst at 400 °C for 30 min of S2p XPS in Fig 6. A single peak located at 168.9 eV attributed to “inorganic” sulfate with ionic S=O bands was observed in Cu/SAPO-34-SA and Cu/SAPO-34-HSA sample, revealing surface sulfur species in the form of SO_4^{2-} was presented.[42, 43] In contrast, sulfur species was insignificant on spent Cu/SAPO-34 catalyst after testing SCR activity of the Cu/SAPO-34-F catalyst at 400 °C for 30 min, revealing that the relative amount of sulfate did

not obviously increase in 30min. This further verified the stability of the catalyst and its activity in SO_2-contaning gas at high temperature.

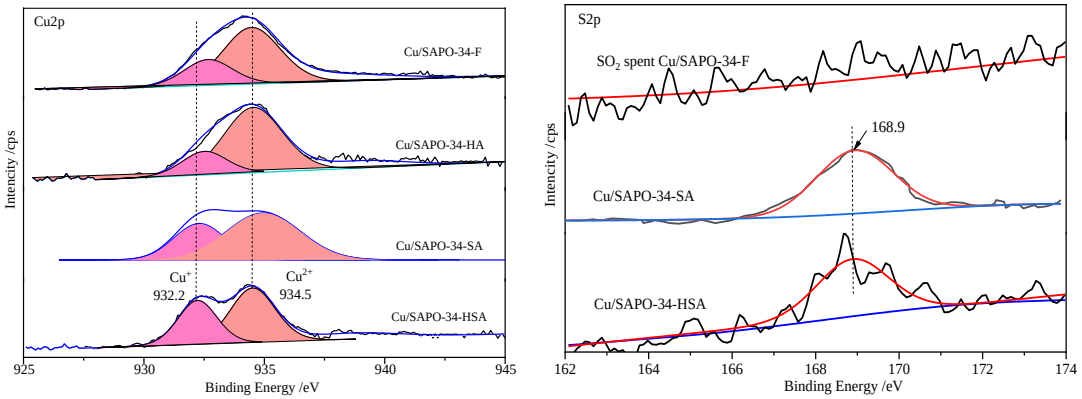

Figure 6. Cu2p and S2p XPS of the Cu/SAPO-34 samples before and after various treatments.

Table 3 Cu2p XPS curve-fitting results on the surface of the samples (%).

Samples	Cu^{2+}	Cu^{+}
	934. eV	932.2eV
Cu/SAPO-34-F	88.6	11.4
Cu/SAPO-34-HA	89.1	10.9
Cu/SAPO-34-SA	67.5	32.5
Cu/SAPO-34-HSA	68	32

3.4 Identification of Sulfate Species. 3.4.1 TGA-DTG-DSC. The TGA-DTG-DSC profiles of the fresh Cu/SAPO-34-F and aged catalysts were shown in Fig. 7. The first weight loss occurred below 200 °C from TGA, which can be attributed to water evaporation.[18, 41, 42] The mass fraction of fresh Cu/SAPO-34 catalyst decreased to 95.4% at 200 °C and continuedly decreased a further 1.4 % between 200°C and 800 °C, indicating that fresh Cu/SAPO-34 catalyst has good thermal stability. The mass fraction of Cu/SAPO-34-HA catalyst reduced by 21.2 % at 200 °C, which indicated that the Cu/SAPO-34 catalyst has strong adsorption capacity for water. But as the temperature went, the mass fraction decreased slightly by about 1.2 % between 300 and 400 °C and kept stable over 400 °C. The weight loss of Cu/SAPO-34-SA was slight with 5.8 % below 200 °C and further decreased between 600 °C and 790 °C with the weight loss decrease of 1.4 %. The weight loss rate of Cu/SAPO-34-HSA was significantly higher than Cu/SAPO-34-F, but lower than that Cu/SAPO-34-HA below 200°C. However, the mass fraction of Cu/SAPO-34-HSA continued to decline of 5.3 % between 200 and 580 °C, indicating sulfate formed. Moreover, the third weight loss was observed between 600 and 790 °C with the weight loss decrease of 5.5 %.

From DTG curve, a peak at around 100-115 °C can be seen for all samples due to water evaporation. It is noted that there were another three peaks at 375, 625 and 750 °C on the DTG curve of Cu/SAPO-34-HSA sample, which is accompanied with two obvious weight loss peaks on TGA curve. According to the decomposition temperature of sulfate, the weight loss is ascribed to the decomposition of S species and metal sulfate species (Al-sulfate, Cu-sulfate).[12, 41] As it is reported that a significantly larger amount of copper sulfates was detected in a humid environment, and more stable sulfate species were produced in the presence of H_2O and O_2 by Wijayanti *et al.*[39] As the metal-sulfate usually decomposes at 600−800 °C,[24] the curve was stable after 750 °C, indicating that sulfate has been completely decomposed. The thermal stability of all catalysts was further conducted by DSC analysis in Fig. 7b. An endothermic peak at around 98-114 °C can be seen with H_2O desorption for all samples. For Cu/SAPO-34-HSA catalyst, another two exothermic peaks at 410 °C and 610 °C owe to S-containing species (eg. Cu-HSO_3, H_2SO_4 species),[43, 44] and the CuO decomposition reaction ($CuO \rightarrow Cu^0$).[42] In addition, the endothermic peak at 740 °C was the decomposition and desorption of metal sulfate species,[41, 45] which was in line with the results of TGA-DTG.

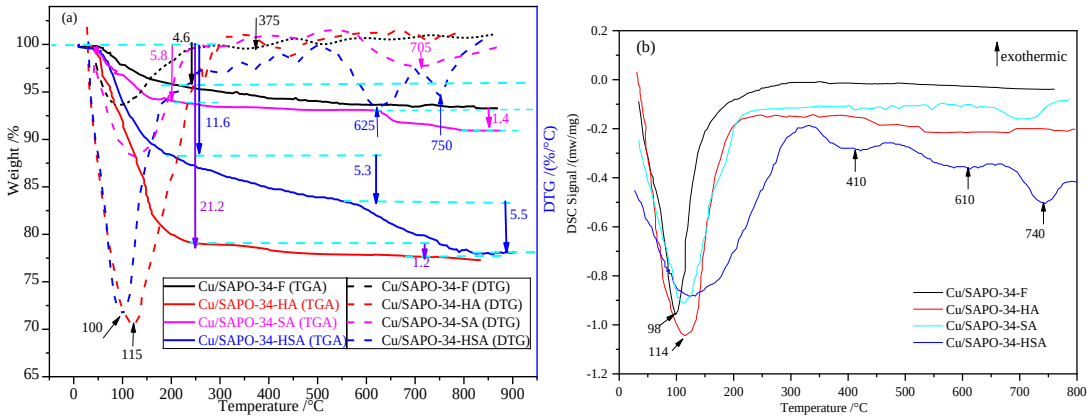

Figure 7. TGA-DTG(a)-DSC(b) curves of the thermal decomposition for various samples

3.5 DFT Calculations. 3.5.1 SO_2 Adsorption. SO_2 adsorption behavior on four different Cu species of Cu/SAPO-34 catalyst was investigated. On the basis of DFT results, shown in Fig. 8 and Table 4, SO_2 was much more likely to interact with four Cu species by its O end (*OSO structure) than the S atom (*SO_2 structure), indicating that the S atom can weakly interact with the Cu species which was consistent with the previous result.[7] The calculation results indicated the adsorption of SO_2 (*OSO) on the CuO species was the strongest (exothermic by 0.62 eV) with the bond length of the Cu−O(SO_2) bond of 2.32 Å. A slightly weaker interaction between CuO and S atom would form

with an adsorption energy of −0.18 eV and the length of the Cu−S bond was 3.18 Å. The other three Cu species showed limited interaction with both the O and S atoms of SO_2. The adsorption of SO_2 on the Cu^{2+} ions in 6MR and 8MR were weakly exothermic by 0.17 eV and 0.23 eV, respectively. Similar results occurred in the Cu^{+} ions with the length of the Cu−S bond of 3.09 Å and an adsorption energy of -0.17 eV. It was indicated that Cu^{2+}(in 6MR/8MR) and Cu^{+} were not the favorable sites for SO_2 adsorption, whereas SO_2 tends to adsorb on CuO sites leading to the formation of the stable bisulfite/bisulfate species. This was consistent with the result of H_2-TPR with less CuO observed on Cu/SAPO-34-SA.

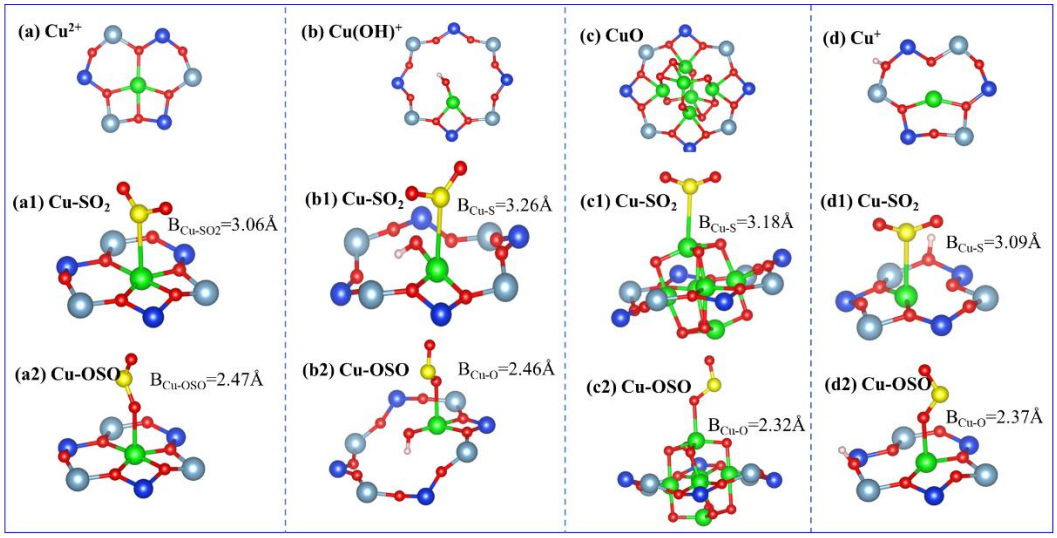

Figure 8. Local structures and bond lengths for the adsorption of SO_2 on (a) Cu^{2+}, (b) $Cu(OH)^{+}$, (c) CuO and (d) Cu^{+}. Red, blue, gray, green and pink spheres correspond to O, Si, Al, Cu, and H atoms, respectively.

Table 4 Calculated Cu–SO_2 Adsorption Energies and Bond Lengths.

Cu species	Adsorption energies (eV)		Bond lengths (Å)	
	*SO_2	*OSO	*SO_2	*OSO
Cu^{2+}	-0.17	-0.40	3.06	2.47
$Cu(OH)^{+}$	-0.23	-0.47	3.26	2.46
CuO	-0.18	-0.62	3.18	2.32
Cu^{+}	-0.17	-0.45	3.09	2.37

3.5.2 Reaction of SO_2 with O_2 on Cu Species. Based on the above results, the energy barriers and energy changes of the reactions between Cu species and SO_2 by starting from the adsorption of SO_2 (*OSO) on Cu species, and the relative energy diagrams were shown in Fig. 9. As shown in Fig. 9a-d, the adsorption of SO_2 on the Cu^{2+} sites in 6MR was exothermic by 0.4 eV, but a slight energy (0.17 eV) needed to be consumed for the following adsorption of O_2 on the isolated Cu^{2+}

ion. The transition state appeared after consuming an energy barrier of 0.52 eV. Then the original Cu site was recovered, and sulfur trioxide was released from an immediate species of the sulfate-like species Cu−SO_4 complex. The release of SO_3 is an endothermic reaction process. The total energy for the escape of SO_3 out of the Cu−SO_4 complex on isolated Cu^{2+} in 6MR was 0.79 eV. The sulfur poisoning on $Cu(OH)^+$, CuO and Cu^+ species showed a similar reaction pathway with 0.32, 2.39 and 1.79 eV for the escape of SO_3, respectively, as shown in Fig. 9b-d. So the energy barrier for the desulfation process was CuO > Cu^+ > Cu^{2+} > $Cu(OH)^+$ sites. The dissociation of SO_3 played an important role in resistance to SO_2 poisoning.[22] The energy barrier for the desulfation process on $Cu(OH)^+$ sites was lowest. These calculation results suggested SO_2 can readily bond with the site of CuO species, which generated stable sulfate-like species Cu−SO_4 complex, whereas sulfate-like species was easy to decompose with the escape of SO_3 from the sites of $Cu(OH)^+$. It was indicated that CuO was a favorable site for SO_2 adsorption and sulfate, while $Cu(OH)^+$ sites in 8MR was not easy to be poisoned by easily releasing SO_3. It should be noted that it is also a little difficult to release SO_3 from the Cu−SO_4 complex once SO_2 adsorb on Cu^+ sites. As reports suggested that SO_2 tends to adsorb on Cu^+ and Cu^+/H^+ sites compared with isolated Cu^{2+}.[7, 21]

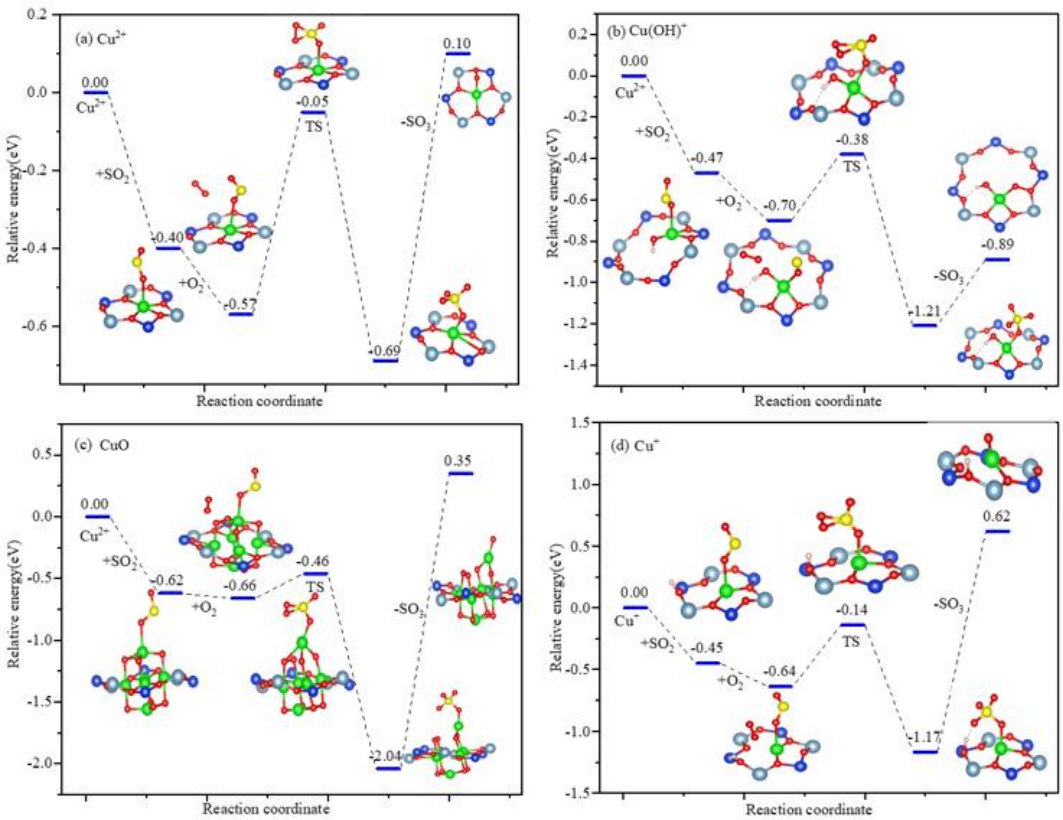

Figure 9. Energy diagrams for the reaction of SO_2 on (a) Cu^{2+}, (b) $Cu(OH)^+$, (c) CuO and (d) Cu^+

sites. Local structures were inserted.

4. SUMMARY AND CONCLUSIONS

In this study, four Cu species including isolated Cu^{2+} in 6MR, $Cu(OH)^{+}$ in 8MR, CuO and Cu^{+} sites on Cu/SAPO-34 were observed and investigated to determine their behaviour toward hydrothermal aging and sulfur poisoning. The catalytic performance of the fresh Cu/SAPO-34 sample was more severely affected by the sulfur poisoning treatment than hydrothermal aging. The high temperature hydrothermal aging had no detectable influence on the integrity of the SAPO-34 framework while SO_2 poisoning during medium temperature hydrothermal aging was observed to 'dealuminate' framework Al^{3+} ions and lead to the formation of $CuAlO_x$ species, which are difficult to reduce and therefore unable to partake in the NH_3-SCR reaction. This is particularly notable in the samples that had undergone hydrothermal aging and SO_2 poisoning. Consequently and/or coincidentally, $Cu(OH)^{+}$ initially present in the 8MR tend to migrate into the 6MR and even agglomerate to form CuO nanoparticles during SO_2 treatment and hydrothermal aging. The interaction of the various Cu species with SO_2 resulted in the formation of ammonium bisulfate and metal bisulfate/sulfates. DFT calculations indicated that the $Cu(OH)^{+}$ site in 8MR was more resistant to SO_2 poisoning than Cu^{2+} in 6MR, CuO and Cu^{+} sites owing to its tendency to release SO_3 easily.

In conclusion we observe that SO_2 is particularly problematic for the performance of Cu/SAPO-34 NH_3-SCR catalysts leading to the loss of Cu species active for NO mitigation, the combination with hydrothermal aging leading to the formation of $CuAlO_x$ species having likely further implications on the structural integrity of the porous material. Mitigating this problem requires upstream solutions i.e. the use of low sulfur fuel/lubricants and possible sulfur traps before the SCR technology.

ASSOCIATED CONTENT

Supporting Information

The Supporting Information is available free of charge at.

Additional N_2 selectivity, Copper speciation analysis via EPR spectra and UV–vis spectrum, and Local structures of Cu/SAPO-34 sample by DFT.

AUTHOR INFORMATION

Corresponding Authors

Boxiong Shen-Tianjin Key Laboratory of Clean Energy and Pollution Control, School of Energy and Environmental Engineering, Hebei University of Technology, Tianjin 300401, China. E-mail: shenbx@hebut.edu.cn

Andrew M. Beale-Chemistry Department, University College London, London WC1H 0AJ, U.K & Research Complex at Harwell, Rutherford Appleton Laboratory, Harwell Science and Innovation Campus, Harwell, Didcot, Oxon, OX11 0FA, U.K

E-mail: andrew.beale@ucl.ac.uk

Authors

Fumei Wang-Tianjin Key Laboratory of Clean Energy and Pollution Control, School of Energy and Environmental Engineering, Hebei University of Technology, Tianjin 300401, China.

Qi Cai-Tianjin Key Laboratory of Clean Energy and Pollution Control, School of Energy and Environmental Engineering, Hebei University of Technology, Tianjin 300401, China.

Xinhua He-Tianjin Key Laboratory of Clean Energy and Pollution Control, School of Energy and Environmental Engineering, Hebei University of Technology, Tianjin 300401, China.

Leila Negahdar-School of Chemistry, University College Dublin, Bellfield, Dublin D04 N2E5, Ireland.

Feng Shuo-Tianjin Key Laboratory of Clean Energy and Pollution Control, School of Energy and Environmental Engineering, Hebei University of Technology, Tianjin 300401, China.

Authors Contributions

Fumei Wang: Project administration, Methodology, Writing–original draft. **Qi Cai**: Investigation, Writing–original draft, Methodology, Validation. **Xinhua He**: Investigation, Methodology, Validation. **Boxiong Shen**: Supervision, Conceptualization, Data curation, Funding acquisition. **Leila Negahdar**: Writing-review & editing. **Feng Shuo**: Investigation, Methodology, Validation. **Andrew M. Beale**: Supervision, Writing - review & editing.

Conflicts of interest

The authors declare no competing financial interest.

ACKNOWLEDGMENTS

The work was supported by Joint Fund of the National Natural Science Foundation of China (U20A20302), the Natural Science Foundation of Hebei Province(E2022202188),

Innovative group projects in Hebei Province (E2021202006, 22554001D), Key R & D projects in Tianjin (19ZXSZSN00050, 19ZXSZSN00070), Key R & D projects in Hebei Province (20373701D), Project of great transformation of scientific and technical research in Hebei Province (21283701Z).

REFERENCES

(1) A.M. Beale, F. Gao, I. Lezcano-Gonzalez, C. Peden, J. Szanyi, C.S. Reviews, Recent advances in automotive catalysis for NOx emission control by small-pore microporous materials, Chem. Soc. Rev. 44 (20) (2015) 7371-7405. https://doi.org/10.1039/c5cs00108k.

(2) J. Woo, D. Bernin, H. Ahari, M. Shost, M. Zammit, L. Olsson, Understanding the mechanism of low temperature deactivation of Cu/SAPO-34 exposed to various amounts of water vapor in the NH_3-SCR reaction, Catal. Sci. Technol. 9 (14) (2019) 3623-3636. https://doi.org/10.1039/c9cy00240e.

(3) S. Zhang, Y. Meng, K. C. Kemp, C. Pan, Q. Ding, L. Pang, W. Cai, T. Li, Revealing the mechanism differences of diverse strategies in boosting the low-temperature hydrothermal durability of Cu-SAPO-34 NH_3-SCR catalysts, Chemical Engineering Journal 452 (2023) 139143. https://doi.org/10.1016/j.cej.2022.139143.

(4) L. Negahdar, N.E. Omori, M.G. Quesne, M.D. Frogley, F. Cacho-Nerin, W. Jones, S.W.T. Price, C.R.A. Catlow, A.M. Beale, Elucidating the significance of copper and nitrate speciation in Cu-SSZ-13 for N_2O formation during NH_3-SCR, ACS Catal. 11 (21) (2021) 13091-13101. https://doi.org/10.1021/acscatal.1c03174.

(5) Aiyong Wang, Ying Chen, Eric D. Walter Nancy M. Washton, Donghai Mei, Tamas Varga, Yilin Wang, János Szanyi, Yong Wang, Charles H.F. Peden, Feng Gao, Unraveling the mysterious failure of Cu/SAPO-34 selective catalytic reduction catalysts, Nature Communications, (2019) 10:1137.

(6) Susanna L. Bergman, Sandra Dahlin, Vitaly V. Mesilov, Yang Xiao, Johanna Englund, Shibo Xi, Chunhua Tang, Magnus Skoglundh, Lars J. Pettersson, Steven L. Bernasek, In-situ studies of oxidation/reduction of copper in Cu-CHA SCR catalysts: Comparison of fresh and SO_2-poisoned catalysts, Applied Catalysis B: Environmental 269 (2020) 118722.

(7) G. Yang, X. Du, J. Ran, X. Wang, Y. Chen, L. Zhang, Understanding SO_2 poisoning over different copper species of Cu-SAPO-34 catalyst: A periodic DFT study, J. Phys. Chem. C 122 (37)

(2018) 21468-21477. https://doi.org/10.1021/acs.jpcc.8b06765.

(8) L. Zhang, D. Wang, Y. Liu, K. Kamasamudram, J.H. Li, W. Epling, SO_2 poisoning impact on the NH_3-SCR reaction over a commercial Cu-SAPO-34 SCR catalyst, Appl. Catal. B 156-157 (2014) 371-377. https://doi.org/10.1016/j.apcatb.2014.03.030.

(9) J.Y Luo, D. Wang, A. Kumar, J.H Li, K. Kamasamudram, N. Currier, A. Yezerets, Identification of two types of Cu sites in Cu/SSZ-13 and their unique responses to hydrothermal aging and sulfur poisoning, Catal. Today 267 (2016) 3-9. https://doi.org/10.1016/j.cattod.2015.12.002.

(10)D.W. Brookshear, J.G. Nam, K. Nguyen, T.J. Toops, A. Binder, Impact of sulfation and desulfation on NOx reduction using Cu-chabazite SCR catalysts, Catal. Today 258 (2015) 359-366. https://doi.org/10.1016/j.cattod.2015.04.029.

(11) Y. Jangjou, D. Wang, A. Kumar, J.H Li, W.S. Epling, SO_2 Poisoning of the NH_3-SCR Reaction over Cu-SAPO-34: Effect of Ammonium Sulfate versus Other S-Containing Species, ACS Catal. 6 (10) (2016) 6612-6622. https://doi.org/ 10.1021/acscatal.6b01656.

(12) P.S. Hammershøi, Y. Jangjou, W.S. Epling, A.D. Jensen, T.V.W. Janssens, Reversible and irreversible deactivation of Cu-CHA NH_3-SCRcatalysts by SO_2 and SO_3, Appl. Catal. B 226 (2018) 38-45. https://doi.org/10.1016/j.apcatb.2017.12.018.

(13) K. Leistner, L. Olsson, Deactivation of Cu/SAPO-34 during low-temperature NH_3-SCR, Appl. Catal. B 165 (2015) 192-199. https://doi.org/10.1016/j.apcatb.2014.09.067.

(14) Y. Jangjou, Q. Do, Y.T. Gu, L.G. Lim, H. Sun, D. Wang, A. Kumar, J.H. Li, L.C. Grabow, W.S. Epling, Nature of Cu Active Centers in Cu-SSZ-13 and Their Responses to SO_2 Exposure, ACS Catal. 8 (2) (2018) 1325-1337. https://doi.org/10.1021/acscatal.7b03095.

(15) A.Y. Wang, L. Olsson, Insight into the SO_2 poisoning mechanism for NOx removal by NH_3-SCR over Cu/LTA and Cu/SSZ-13, Chem. Eng. J. 395 (2020). 125048. https://doi.org/10.1016/j.cej.2020.125048.

(16) H. Wang, H. Li, L. Gao, X. Tian, J. Hao, P. Ning, J. Chen, Q. Zhang, Pr-functionalized Cu/SAPO-34 with superior hydrothermal stability for NH_3-SCR: The copper species and framework stabilization effect, Fuel 327 (2022) 125229. https://doi.org/10.1016/j.fuel.2022.125229.

(17) A.J. Shih, I. Khurana, H. Li, J. González, A. Kumar, C. Paolucci, T.M. Lardinois, C.B. Jones, J.D.A. Caballero, K. Kamasamudram, A. Yezerets, W.N. Delgass, J.T. Miller, A.L. Villa, W.F. Schneider, R. Gounder, F.H. Ribeiro, Spectroscopic and kinetic responses of Cu-SSZ-13 to SO_2

exposure and implications for NOx selective catalytic reduction, Appl Catal A-gen. 574 (2019) 122-131. https://doi.org/10.1016/j.apcata.2019.01.024.

(18) C. Wang, J. Wang, J.Q. Wang, T. Yu, M.Q. Shen, W.L. Wang, W. Li, The effect of sulfate species on the activity of NH_3-SCR over Cu/SAPO-34, Appl. Catal. B 204 (2017) 239-249. https://doi.org/10.1016/j.apcatb.2016.11.033.

(19)Y.D. Tang, D. Wang, X. Wang, Y.H. Zha, H.M. An, K. Kamasamudram, A. Yezerets, Impact of low temperature sulfur exposure on the aging of small pore Cu-zeolite SCR catalyst, Catal. Today 360 (2021) 234-240. https://doi.org/10.1016/j.cattod.2020.04.033.

(20)X. Yong, C.J. Zhang, M. Wei, P.P. Xie, Y.D. Li, Promotion of the performance of Cu-SSZ-13 for selective catalytic reduction of NOx by ammonia in the presence of SO_2 during high temperature hydrothermal aging, J. Catal. 394 (2021) 228-235. https://doi.org/10.1016/j.jcat.2020.06.041.

(21)P.S. Hammershøi, P.N.R. Vennestrøm, H. Falsig, A.D. Jensen, T.V.W. Janssens, Importance of the Cu oxidation state for the SO_2-poisoning of a Cu-SAPO-34 catalyst in the NH_3-SCR reaction, Appl. Catal. B 236 (2018) 377-383. https://doi.org/10.1016/j.apcatb.2018.05.038.

(22) P.R. Chen, A. Khetan, M. Jabłońska, J. Simböck, M. Muhler, R. Palkovits, H. Pitsch, U. Simon, Local dynamics of copper active sites in zeolite catalysts for selective catalytic reduction of NOx with NH_3, Appl. Catal. B 237 (2018) 263-272. https://doi.org/10.1016/j.apcatb.2018.05.091.

(23) S. Zhang, Y. Meng, L. Pang, Q. Ding, Z. Chen,Y. Guo, W. Cai, T. Li, Understanding the direct relationship between various structure-directing agents and low temperature hydrothermal durability over Cu-SAPO-34 during the NH_3-SCR reaction, Catal. Sci. Technol., 2022,12, 579. https://doi.org/10.1039/d1cy02046c.

(24) L. Wei, D.W. Yao, F. Wu, B. Liu, X.H. Hu, X.W. Li, X.L. Wang, Impact of Hydrothermal Aging on SO_2 Poisoning over Cu-SSZ-13 Diesel Exhaust SCR Catalysts, Ind. Eng. Chem. Res. 58 (10) (2019) 3949-3958. https://doi.org/10.1021/acs.iecr.8b04543.

(25)X.H. Li, Y.N. Zhao, H.W. Zhao, M.K. Liu, Y.H. Ma, X. Yong, H. Chen, Y.D. Li, The Cu migration of Cu-SAPO-34 catalyst for ammonia selective catalytic reduction of NOx during high temperature hydrothermal aging treatment, Catal. Today 327 (2019) 126-133. https://doi.org/10.1016/j.cattod.2018.05.029.

(26) Hailong Zhang, Jianhang Lv, Zhun Zhang, Congcong Du, Shuai Wang, Jingdong Lin, Shaolong Wan, Yong Wang, Haifeng Xiong. Oxidation of Methane to Methanol by Water Over Cu/SSZ-13:

Impact of Cu Loading and Formation of Active Sites, ChemCatChem 14(2022)e202101609. https://doi.org/10.1002/cctc.202101609

(27) Aiyong Wang, Ying Chen, Eric D. Walter Nancy M. Washton, Donghai Mei, Tamas Varga, Yilin Wang, János Szanyi, Yong Wang, Charles H.F. Peden, Feng Gao, Unraveling the mysterious failure of Cu/SAPO-34 selective catalytic reduction catalysts, Nature Communications, (2019) 10:1137.

(28) Y. Shan, X. Shi, Z. Yan, J. Liu, Y. Yu, H. He, Deactivation of Cu-SSZ-13 in the presence of SO_2 during hydrothermal aging, Catal. Today 320 (2019) 84-90. https://doi.org/10.1016/j.cattod.2017.11.006.

(29)J. Cheng, S. Han, Q. Ye, S.Y. Cheng, T.F. Kang, H.X. Dai, Selective catalytic reduction of NO with NH_3 over the Cu/SAPO-34 catalysts derived from different Cu precursors, Micropor Mesopor Mat. 278 (2019) 423-434. https://doi.org/10.1016/j.micromeso.2019.01.013.

(30)M.H. Xu, J. Wang, T. Yu, J.Q. Wang, M.Q. Shen, New insight into Cu/SAPO-34 preparation procedure: Impact of NH_4-SAPO-34 on the structure and Cu distribution in Cu-SAPO-34 NH_3-SCR catalysts, Appl. Catal. B 220 (2018) 161-170. https://doi.org/10.1016/j.apcatb.2017.08.031.

(31) Y. Cao, D. Fan, L.J. Sun, M. Yang, L. Cao, T.T. Sun, S.T. Xu, P. Tian, Z.M. Liu, The self-protection effect of reactant gas on the moisture stability of CuSAPO-34 catalyst for NH_3-SCR, Chem. Eng. J. 374 (2019) 832-839. https://doi.org/10.1016/j.cej.2019.05.227.

(32) S. Han, J. Cheng, Q. Ye, S.Y. Cheng, T.F. Kang, H.X. Dai, Ce doping to Cu-SAPO-18: enhanced catalytic performance for the NH_3-SCR of NO in simulated diesel exhaust, Micropor Mesopor Mat. 276 (2019) 133-146. https://doi.org/10.1016/j.micromeso.2018.09.027.

(33) H. Jiang, B. Guan, H. Lin, Z. Huang, Cu/SSZ-13 zeolites prepared by in situ hydrothermal synthesis method as NH3-SCR catalysts: Influence of the Si/Al ratio on the activity and hydrothermal properties, Fuel 255 (2019) 115587. https://doi.org/10.1016/j.fuel.2019.05.170.

(34) B.H. Chen, R.N. Xu, R.D. Zhang, N. Liu, Economical way to synthesize SSZ-13 with abundant ion-exchanged Cu^+ for an extraordinary performance in selective catalytic reduction (SCR) of NOx by ammonia, Environ. Sci. Technol. 48 (23) (2014) 13909-13916. https://doi.org/10.1021/es503707c.

(35) H.Y. Tian, Y. Ping, Y.B. Zhang, Z.S. Zhang, L.W. Sun, P. Liu, J.J. Zhu, X.G. Yang, Atomic layer deposition of silica to improve the high-temperature hydrothermal stability of Cu-SSZ-13 for

NH_3 SCR of NOx, J. Hazard. Mater. 416 (2021) 126194. https://doi.org/10.1016/j.jhazmat.2021.126194.

(36) J.C. Wang, Z.Q. Liu, G. Feng, L.P. Chang, W.R. Bao, In situ synthesis of CuSAPO-34/cordierite and its selective catalytic reduction of nitrogen oxides in vehicle exhaust: The effect of HF, Fuel 109 (2013) 101-109. https://doi.org/10.1016/j.fuel.2012.09.046.

(37)C. Fan, Z. Chen, L. Pang, S.J. Ming, C.Y. Dong, K.B. Brou Albert, P. Liu, J.Y. Wang, D.J. Zhu, H.P. Chen, T. Li, Steam and alkali resistant Cu-SSZ-13 catalyst for the selective catalytic reduction of NOx in diesel exhaust, Chem. Eng. J. 334 (2018) 344-354. https://doi.org/10.1016/j.cej.2017.09.181.

(38)P.R. Chen, V. Rizzotto, A. Khetan, K.P. Xie, R. Moos, H. Pitsch, D.Q. Ye, U. Simon, Mechanistic understanding of Cu-CHA catalyst as sensor for direct NH_3-SCR monitoring: the role of Cu mobility, ACS Appl. Mater. Interfaces 11 (8) (2019) 8097-8105. https://doi.org/10.1021/acsami.8b22104.

(39) K. Wijayanti, K.P. Xie, A. Kumar, K. Kamasamudram, L. Olsson, Effect of gas compositions on SO_2 poisoning over Cu/SSZ-13 used for NH_3-SCR, Appl. Catal. B 219 (2017) 142-154. https://doi.org/10.1016/j.apcatb.2017.07.017.

(40)G.L. Li, Q. Wu, S.X. Wang, J.H. Li, X.Q. You, S. Shao, M.N. Wen, L.W. Xu, Y. Tang, F.Y. Wang, Y. Wang, K.Y. Liu, Promoting SO_2 resistance of a CeO_2(5)-WO_3 (9)/TiO_2 catalyst for Hg^0 oxidation via adjusting the basicity and acidity sites using a CuO doping method, Environ. Sci. Technol. 54 (3) (2020) 1889-1897. https://doi.org/10.1021/acs.est.9b04465.

(41) M.Q. Shen, Y. Zhang, J.Q. Wang, C. Wang, J. Wang, Nature of SO_3 poisoning on Cu/SAPO-34 SCR catalysts, J. Catal 358 (2018) 277-286. https://doi.org/10.1016/j.jcat.2017.12.008.

(42)L. Wang, J.R. Gaudet, W. Li, D. Weng, Migration of Cu species in Cu/SAPO-34 during hydrothermal aging, J. Catal 306 (2013) 68-77. https://doi.org/10.1016/j.jcat.2013.06.010.

43)J.P. Du, X.Y. Shi, Y.L. Shan, G.Y. Xu, Y. Sun, Y.J. Wang, Y.B. Yu, W.P. Shan, H. He, Effects of SO_2 on Cu-SSZ-39 catalyst for the selective catalytic reduction of NOx with NH_3, Catal. Sci. Technol. 10 (5) (2020) 1256-1263. https://doi.org/10.1039/c9cy02186h.

(44) W.K. Su, Z.G. Li, Y.N. Zhang, C.C. Meng, J.H. Li, Identification of sulfate species and their influence on SCR performance of Cu/CHA catalyst, Catal. Sci. Technol. 7 (7) (2017) 1523-1528. https://doi.org/10.1039/c7cy00302a.

(45)H. Armendariz, B. Coq, D. Tichit, R. Dutartre, F. Figu´eras, Influences of some synthesis parameters and activation procedures on the one-step sol – gel synthesis of sulfated-zirconia catalysts, followed by TG-DSC and mass spectrometry, J. Catal 173 (2) (1998) 345 – 354. https://doi.org/10.1006/jcat.1997.1926.

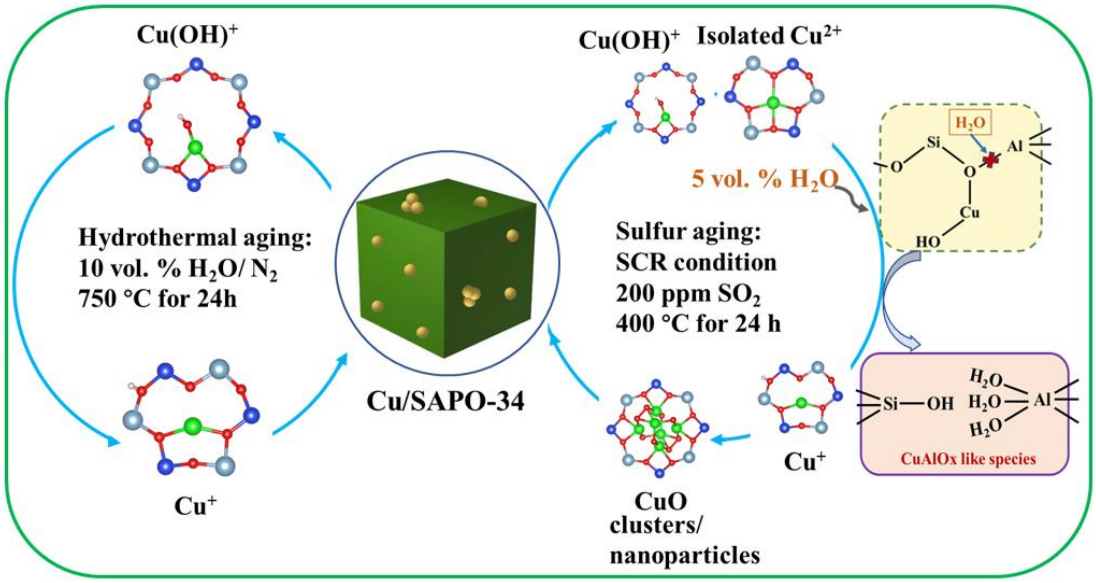

Table of Contents Image